

Statistical Hadronization Probed by Resonances

Giorgio Torrieri and Johann Rafelski

Department of Physics, University of Arizona, Tucson, Arizona 85721, USA

(Dated: May, 2003)

We study to what extent a measurement of the m_{\perp} spectra for hadrons and their resonances can resolve ambiguities in the statistical model description of particle production. We describe in a quantitative analysis how physical assumptions about the freeze-out geometry and dynamics influence the particle spectra. Considering ratios of m_{\perp} distribution of resonance-particle ratios (such as K^*/K , Σ^*/Λ , η'/η) we observe significant sensitivity to fireball freeze-out geometry and flow dynamics.

PACS number(s): 12.38.Mh, 25.75.-q, 24.10.Pa

I. INTRODUCTION

The Fermi statistical model of particle production [1, 2, 3, 4] has been used extensively in the field of relativistic heavy ion collisions [5]. Particle abundancies and spectra both at Super Proton Synchrotron (SPS) [6, 7, 8, 9, 10, 11, 12] and Relativistic Heavy Ion Collider (RHIC) [13, 14, 15, 16, 17, 18] energies have been analyzed in this way. The quality of fits to experimental results was such that it became possible to discuss hadronization conditions quantitatively, but the conclusions of the groups differ. For example the values of temperature range from as low as 110 MeV [9, 14, 15, 16] to 140 MeV [10, 13] to as high as 160, 170, and 180 MeV [6, 8, 11, 15, 17, 18] at both SPS and RHIC energies.

These differences are on a closer inspection not very surprising, since the (tacit) assumptions made about hadronization mechanisms differ. However, this means that before we can say that the freeze-out temperature has been determined, we must understand precisely the origins of these differences, and proceed to ascertain which model is applicable. We shall suggest experimental observables which will be particularly sensitive to the differences between the hadronization scenarios, in the hope that further experimental study will allow to understand the statistical hadronization mechanism.

We begin with an overview of the differences between hadronization scenarios and their relation to the physical assumptions used. Every model discussed here has been extensively studied before, and has gained acceptance of some part of the heavy ion community. The theoretical principles that we invoke are well understood, and the methods we use can be found scattered in literature. We shall concentrate here on an analysis of resonances produced in a heavy ion collision. Direct detection of hadronic short-lived resonances has become possible through invariant mass reconstruction [19, 20, 21, 22]. Resonances have already been proposed as candidates for differentiating between freeze-out models [23]. Resonances are a sensitive probe of the freeze-out temperature, since the ratio of yields of particles with the same quark composition is insensitive to both fugacities and phase space occupancies, and mass differences are greater than the hadronization temperature considered.

Here we shall develop this reasoning one step further: If particles were to be emitted from a static thermal source, and feed down corrections were performed, the ratio of resonance to daughter particle would be independent of m_{\perp} . That this ratio is in general somewhat m_{\perp} dependent is in this situation due to dynamical effects, such as hadronizing matter flow and freeze-out geometry. For this reason, it can be expected that the m_{\perp} dependence of this ratio can help isolate these effects and thus remove the ambiguities in the present freeze-out models.

In Sec. II we review hadronization models and discuss their ambiguities. We then show in Sec. III how resonance m_{\perp} ratios can be used to distinguish between particle hadronization models. We close with a short discussion of open issues.

II. STATISTICAL HADRONIZATION

A. General remarks

Nearly all hadronic spectra comprise a significant O(50%) component from resonance decays. Fits to data, which are not allowing for the decay contributions have a very limited usefulness. Particle spectra and thus yields are in general, controlled by the properties of statistical hadronization models. However, some recent work fits the particle slopes only [7, 9, 14, 15], treating the normalization of each particle as a free parameter. This approach can be argued for assuming a long-lived posthadronization “interacting hadron gas phase” in which individual hadron abundances subject to inelastic interactions evolve away from chemical equilibrium. This particular reaction picture clashes with e.g. the fact that short-lived resonance ratios can be described within the statistical hadronization model using the chemical (statistical hadronization) freeze-out temperature obtained in stable particle studies [18]. This implies that in principle the relative normalization of the particle spectra should be derived from a hadronization scenario involving flavor chemical potentials. In fact a study of RHIC spectra finds that the normalization can be accounted for [17], and that the chemical equilibration temperature also describes particle spectra well. This

is suggesting that any posthadronization reinteraction phase is short and has minor influence on the particle yields.

The problem is that the different ways to derive hadronization particle distributions have a profound effect on the resulting fitted temperature. Temperature affects the absolute number of particles through several mechanisms and anticorrelates with the phase space occupancy parameters $\gamma_i, i = u, d, s$ [10, 13]. It has been found that the introduction of these parameters, motivated by the need to conserve entropy at hadronization [13] decrease the χ^2 / per degree of freedom considerably and lowers the freeze-out temperature by 30 MeV [13]. Other workers assume the light flavors are in chemical equilibrium [6, 8, 11, 18].

Considering ratios of resonances to ground state particles eliminates the fitted temperature's sensitivity to chemical equilibration, since the numerator and denominator have the same quark composition. In every hadronization model considered here the chemical parameters cancel out and only temperature and fireball freeze-out geometry and dynamics influence the observed ratios.

When fitting the particle spectra, the system's spatial shape and the way the freeze-out progresses in time have a considerable effect on the form of particle distributions, and hence on the fitted temperature and matter flow. The impact of freeze-out geometry and dynamics on particle spectra were examined well before RHIC data became available [24, 25] and it was realized that an understanding of freeze-out is essential for the statistical analysis of the fireball [26]. Even though this matter has been clearly recognized, a systematic analysis of how freeze-out geometry affects particle distributions is for the first time attempted here. In fact, each of the models used in the study of particle spectra [9, 10, 14, 15, 17] employs a different choice of freeze-out geometry, based on different, often tacitly assumed, hadronization scenarios. Thus an understanding for the influence of hadronization mechanism is impossible to deduce from this diversity.

However, every study of fireball hadronization we are aware of uses the Cooper-Frye formula [27]:

$$E \frac{dN}{d^3p} = \int p^\mu d^3\Sigma_\mu f(p^\mu u_\mu, T, \lambda) \theta(p^\mu d^3\Sigma_\mu), \quad (1)$$

where p^μ is the particle's four-momentum, u^μ is the systems velocity profile, T is the temperature, λ is a chemical potential, $f(E, T, \lambda)$ is the statistical distribution of the emitted particles in terms of energy and conserved quantum numbers and Σ^μ describes the hadronization geometry. It is the covariant generalization of a volume element of the fireball, i.e., a "3D" surface in space-time from which particles are emitted. $\theta(p^\mu d^3\Sigma_\mu)$ is the step function, which eliminates the possible inward emission [28, 29].

The Cooper-Frye formula, Eq. (1), is believed to be the most general way to implement statistical hadronization emission of particles. For it to represent a physical

description of the system, the following two conditions have to be met:

(i) Statistical hadronization must apply. The particles emitted from a volume element (in its co-moving frame), will be distributed according to the Bose-Einstein or Fermi-Dirac distributions $f(E, T, \lambda)$ for some temperature T and fugacity λ .

(ii) A "small" volume element hadronizes rapidly in its rest frame, that is, no long lived mixed Quark gluon plasma (QGP) -hadronic confined phase exists.

If this second condition is satisfied, it becomes possible to define a hadronization hypersurface $\Sigma^\mu = (t_f(x, y, z), x, y, z)$ which specifies at which time t_f hadrons are emitted from the point (x, y, z) . In this fast hadronization case differing Σ^μ can be considered for physically differing models. The different choices of Σ^μ correspond to physically different scenarios, and it becomes possible, in principle, to distinguish them experimentally. However, if a long-lived mixed phase does exist, it might well be that the Cooper-Frye formula can be used as an approximation technique to transform a hydrodynamically evolving system into hadrons and authors who worked with a long mixed phase have chosen this approach, see e.g. Ref. [30].

B. Freeze-out geometry

The high baryon stopping power observed at SPS energies [31, 32, 33] has prompted some authors to use a spherical expansion and freeze-out as an ansatz [10].

However, at RHIC collision energies the measured $dN/d\eta$ [34, 35] indicates that around mid-rapidity the system conditions can be approximated by the Bjorken picture [36].

To describe particle spectra measured around midrapidity, therefore, boost invariance becomes the dominant symmetry on which freeze-out geometry should be based. To construct such a hadronization scenario, we consider that the most general cylindrically symmetric flow profile

$$u^\mu = \begin{pmatrix} \cosh(y_L) \cosh(y_\perp) \\ \sinh(y_\perp) \cos(\theta) \\ \sinh(y_\perp) \sin(\theta) \\ \sinh(y_L) \cosh(y_\perp) \end{pmatrix}, \quad p^\mu = \begin{pmatrix} m_\perp \cosh(y) \\ p_\perp \cos(\phi) \\ p_\perp \sin(\phi) \\ m_\perp \sinh(y) \end{pmatrix} \quad (2)$$

(the last, longitudinal coordinate is defined along the beam direction) leads to the following rest energy [38]:

$$p_\mu u^\mu = m_\perp \cosh(y_\perp) \cosh(y - y_L) - \sinh(y_\perp) \cos(\theta - \phi) p_\perp. \quad (3)$$

The requirement for the Bjorken picture is that the emission volume element has the same y_L dependence:

$$p_\mu d^3\Sigma^\mu \sim A \cosh(y - y_L) + B. \quad (4)$$

This constrains the freeze-out hypersurface to be of the

form

$$\Sigma^\mu = (t_f \cosh(y_L), x, y, t_f \sinh(y_L)). \quad (5)$$

Here t_f is a parameter invariant under boosts in the z direction, whose physical significance depends on the model considered.

For central collisions, a further simplifying constraint is provided by the cylindrical symmetry, which forces t_f , as well as y_L and y_\perp , to be independent of the angles θ and ϕ . The freeze-out hypersurface can be parametrized, in this case, as

$$\Sigma^\mu = (t_f(r) \cosh(y_L), r \sin(\theta), r \cos(\theta), t_f(r) \sinh(y_L)), \quad (6)$$

$$d^3\Sigma^\mu = t_f r dr d\theta dy_L \left(\cosh(y_L) \frac{\partial t_f}{\partial r} \cos(\theta), \frac{\partial t_f}{\partial r} \sin(\theta), \sinh(y_L) \right) \quad (7)$$

And the emission element takes the form

$$p^\mu d^3\Sigma_\mu = \left[m_\perp \cosh(y - y_L) - p_\perp \frac{\partial t_f}{\partial r} \cos(\theta - \phi) \right] t_f r dr d\theta dy_L, \quad (8)$$

with the same dependence on the angle as Eq. (3). Equation (1) can then be integrated over all the possible values of y_L and $\theta - \phi$ to give a particle spectrum depending purely on the transverse mass, temperature, and y_\perp . The fits in [9, 14, 15, 17] are based on such an ansatz.

What distinguishes the models currently considered is the time component of the freeze-out surface. The most general freeze-out hypersurface compatible with cylindrical symmetry is provided by Eq. (6). Generally, t_f (a generic function of r) represents the time, in a frame co-moving with the longitudinal flow, at which the surface at distance r freezes out.

The fits in Refs. [9, 14, 15] are based on a particular case of such a freeze-out surface, in which t_f is completely independent of r ($\partial t_f / \partial r = 0$). Such a picture's physical reasonableness can be questioned, e.g., why should spatially distant volume elements, presumably with different densities and moving at different transverse velocities, all freeze out simultaneously in a longitudinally comoving frame? However, such a simple model can perhaps serve as an approximation.

More generally, the “burning log” model [24, 37] (sometimes referred to as “blast wave”; This term, however, is also used to refer to the $\partial t_f / \partial r = 0$ model described in the preceding paragraph) assumes that the emission occurs through a three-dimensional hadronization surface which is moving at a constant “velocity” ($1/v_f = \partial t_f / \partial r$ throughout the fireball. Both boost-invariant and spherically symmetric versions of burning log model were considered. Even if the hadronization velocity encompasses an extra parameter v_f , it is worth considering since it is based on a physically motivated

hadronization picture. Moreover, the burning log picture is a suitable framework in the study of sudden hadronization. Sudden hadronization occurs when the fireball encounters a mechanical instability [39], which combined with the fireball's high transverse flow ensures that the emission surface spreads to the interior of the fireball with $v_f \simeq c$. All of the indications suggested for such a picture seem to be borne out by both SPS and RHIC data [13, 39, 41].

An approach based on the hypothesis of initial state “synchronization” by the primary instant of collision and the following independent but equivalent evolution of all volume elements assumes that each element of the system undergoes freeze-out at the same proper time τ . In this framework each fireball element expands and cools down independently, hadronizing when its temperature and density reach the critical value. This model was successfully used to describe RHIC m_\perp -spectra [17]. In this approach t_f in Eq. (6) is equal to $\tau \cosh(y_\perp)$ and the hadronization hypersurface in Eq. (7) becomes proportional to the flow vector:

$$\Sigma^\mu = \tau u^\mu \quad (9)$$

$$d^3\Sigma^\mu = \tau r dr d\theta dy_L u^\mu = dV u^\mu \quad (10)$$

$$r = \tau \sinh(y_\perp). \quad (11)$$

In this hadronization model the heavy ion fireball behaves similarly to the expanding Hubble universe. In the ‘Hubble’ scenario, the Cooper-Frye formula reduces to the Touscheck Covariant Boltzmann distribution [5, 38, 43, 44].

$$\frac{V_0 d^3p}{(2\pi)^3} e^{-E/T} \rightarrow \frac{V_\mu p^\mu}{(2\pi)^3} d^4p 2\delta_0(p^2 - m^2) e^{-p_\mu u^\mu / T} \quad (12)$$

$$V^\mu = V_0 u^\mu \quad (13)$$

(Where V is the co moving fireball's volume element in the local rest frame.)

To summarize and illustrate the diversity of distinct hadronization geometries we present in Table I and Fig. 1 the freeze-out scenarios examined here. As we shall see the choice of freeze-out geometry produces in a fit of experimental data a non trivial effect capable of altering significantly the understanding of statistical hadronization parameters.

C. Flow profile

Hydrodynamical expansion of the fireball implies in general that each volume element will have a different density and transverse expansion rate. For this reason, the integral over $d^3\Sigma$ can span a range of flows, weighted by density. In first approximation one can fit data using just an “average” flow velocity throughout the entire

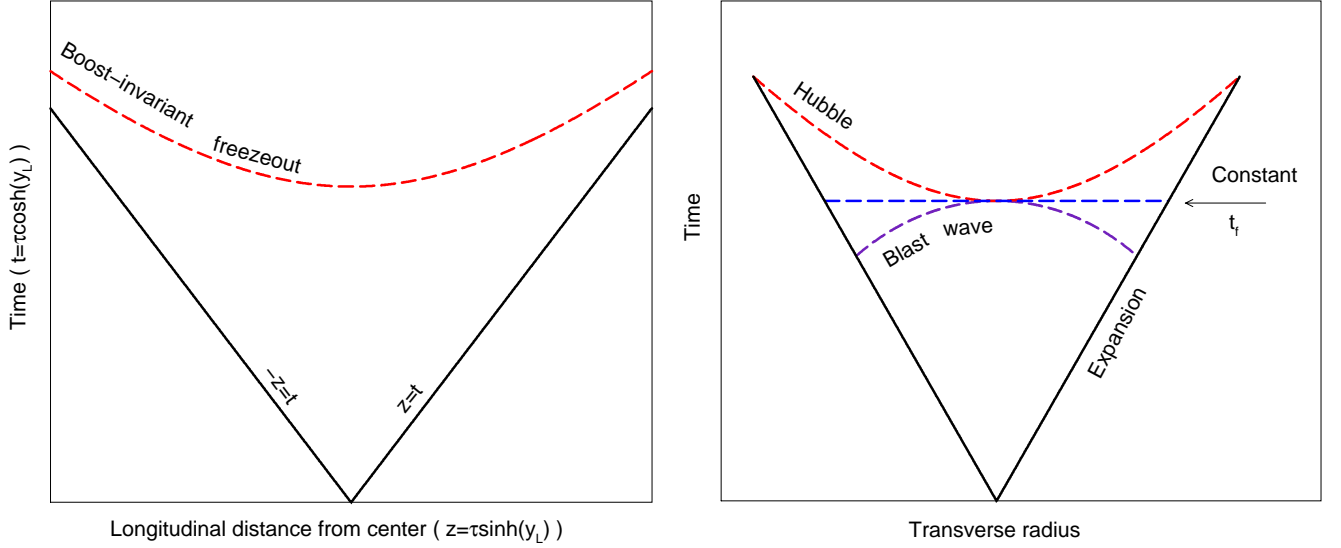


FIG. 1: (Color online) While boost-invariance fixes the longitudinal freeze-out structure (left), several scenarios exist for the transverse dependence of freeze-out (right). For spherical freeze-out, only plot on the right applies

TABLE I: (Color online) Freeze-out hypersurfaces at contours of constant radii.

Surface	Σ^μ	$E \frac{dN}{d^3p}^a$	reference
Constant t_f $\partial t_f / \partial r = 0$	$\begin{pmatrix} t_f \\ \vec{r} \end{pmatrix}$	$m_\perp K_1(\beta m_\perp) I_0(\alpha p_\perp)$	[7, 9, 14, 15, 42]
Hubble (constant τ_f)	$\tau_f \begin{pmatrix} \cosh(y_L) \cosh(y_\perp) \\ \sinh(y_\perp) \cos(\theta) \\ \sinh(y_\perp) \sin(\theta) \\ \sinh(y_L) \cosh(y_\perp) \end{pmatrix}$	$m_\perp \cosh(y_\perp) I_0(\alpha p_\perp) K_1(\beta m_\perp) -$ $p_\perp \sinh(y_\perp) I_1(\alpha p_\perp) K_0(\beta m_\perp)$	[17]
Blast/burning log (boost invariant)	$\begin{pmatrix} t_f(r) \cosh(y_L) \\ r \cos(\theta) \\ r \sin(\theta) \\ t_f(r) \sinh(y_L) \end{pmatrix}$	$m_\perp I_0(\alpha p_\perp) K_1(\beta m_\perp) -$ $p_\perp \frac{\partial t_f}{\partial r} I_1(\alpha p_\perp) K_0(\beta m_\perp)$	This paper, [17]
Blast/burning log (spherical)	$\begin{pmatrix} t_f \\ r \vec{e}_r \end{pmatrix}$	$e^{-E/T} \sqrt{\frac{T}{p_\perp \sinh(y_\perp)}} (E I_{1/2}(\alpha p_\perp) -$ $p_\perp \frac{\partial t_f}{\partial r} I_{3/2}(\alpha p_\perp))$	[10, 24]

$$^a \beta = \cosh(y_\perp)/T, \alpha = \sinh(y_\perp)/T$$

fireball [7, 10]:

$$E \frac{dN}{d^3p} = \int r dr (E - p_\perp \frac{dt_f}{dr}) f(T, y_\perp(r), \lambda) \propto (E - p_\perp \frac{dt_f}{dr}) f(T, \langle y_\perp \rangle, \lambda). \quad (14)$$

However, if one wants to properly identify $\frac{dt_f}{dr}$, the flow profile should be taken into account [45]. Hydrodynamic simulations [30] accompanied by assumption that freeze-out happens when a volume element reaches a critical energy density indicate that the transverse rapidity will depend linearly with the radius i.e. $v_\perp \sim \tanh(r)$. This condition, however, is appropriate for a static freeze-out

and will not in general hold if the freeze-out is sudden. Other flow profiles have been tried in the literature, arising from dynamical hypothesis. For example, the assumption that the freeze-out occurs at the same time t_f results in a quadratic ($v \propto r^2$) flow profile [40], which has also been used recently in fits to data [15]. In the Hubble fireball [17] the freeze-out conditions will also result in a distinctive flow profile. Specifically with $\Sigma^\mu \propto u^\mu$, we have $\gamma v \propto r$.

Density profiles also depend on the assumed initial condition and the equation of state of the expanding QGP. It has been shown [46] that different density choices have a considerable effect on both the temperature and flow fits at SPS energies.

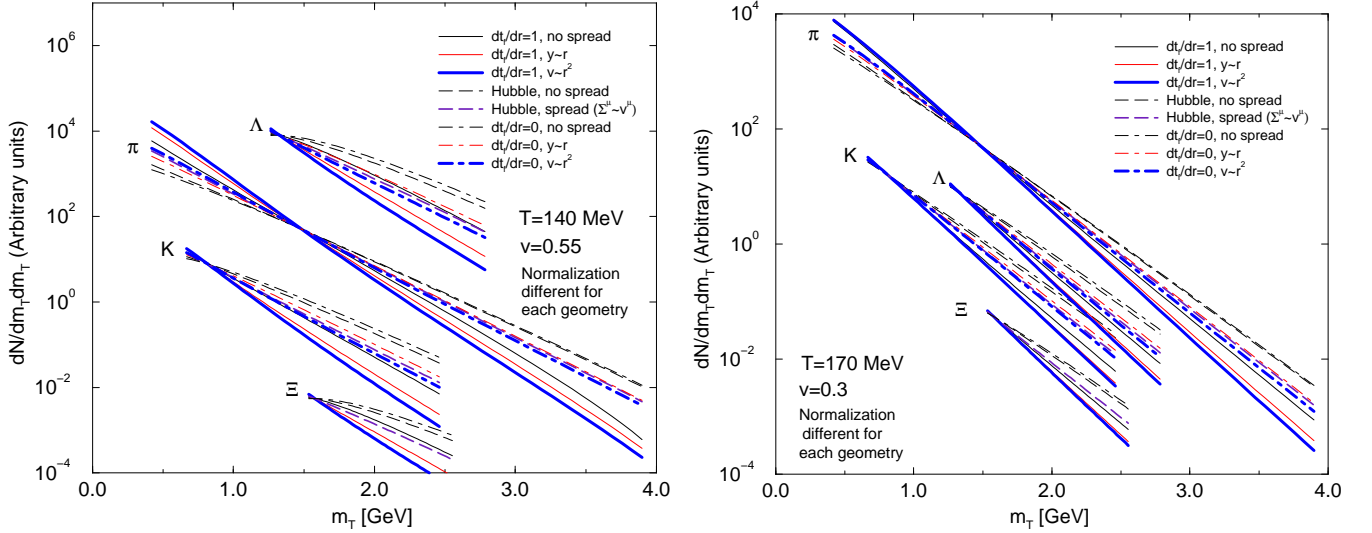


FIG. 2: (Color online) π, K, Λ and Ξ m_{\perp} distributions obtained with different freezeout models and flow profiles. For this and subsequent figures, a uniform density profile was assumed

Figure. 2 shows how the choice in hadronization dynamics and flow profiles at same given freeze-out temperature and transverse flow can result in a range of inverse spectral slopes. Here the density profiles were assumed to be uniform. It is clear that the same freeze-out parameters give rise to a variety of substantially different particle spectra. Conversely, fits to experimental data will only produce reliable information on the freeze-out conditions if and when we have a prior knowledge of the hadronization geometry and dynamics. Therefore, conclusions about statistical model fits, as well as arguments whether freeze-out occurs simultaneously for different particles or not, cannot be answered while the models used to fit the data are plagued by such uncertainties. We will now turn to study how the measurement of spectra of short-lived resonances might provide us with a way of making progress.

III. MOMENTUM DEPENDENCE OF THE RESONANCE-PARTICLE RATIOS AS A FREEZE-OUT PROBE

We have shown that the measurement of resonances can probe both the hadronization temperature, and the lifetime of the interacting hadron gas phase [12, 23]. Ratios of a generic resonance (henceforward called Y^*) to the light particle (which we will refer to as Y) with an identical number of valence quarks are particularly sensitive probes of freezeout temperature because chemical dependence cancels out within the ratio. If we examine this ratio within a given $m_{\perp} > m_{Y^*}$ range, we expect to disentangle flow and freeze-out conditions, since the ratio Y^*/Y should not depend on m_{\perp} for a purely static and thermal source.

We therefore take the most general Boost-invariant

freeze-out hypersurface in the Boltzmann limit (see Table I. Boost invariant implies this is a good approximation at midrapidity)

$$\frac{dN}{dm_T^2} \propto S(m_{\perp}, p_{\perp}) = \int_{\Sigma} r dr \mathcal{S}(m_{\perp}, p_{\perp}, r), \quad (15)$$

where

$$\begin{aligned} \mathcal{S}(m_{\perp}, p_{\perp}, r) = & m_{\perp} K_1(\beta m_{\perp}) I_0(\alpha p_{\perp}) \\ & - \frac{\partial t_f}{\partial r} p_{\perp} K_0(\beta m_{\perp}) I_1(\alpha p_{\perp}), \end{aligned} \quad (16)$$

with

$$\beta = \frac{\cosh[y_{\perp}(r)]}{T}, \quad \alpha = \frac{\sinh[y_{\perp}(r)]}{T} \quad (17)$$

and use it to calculate the ratio between two particles with the same chemical composition. The chemical factors cancel out, and we are left with

$$\frac{Y^*}{Y} = \left(\frac{g^*}{g} \right) \frac{S(m_{\perp}, p_{\perp}^*)}{S(m_{\perp}, p_{\perp})}, \quad (18)$$

where g^* and g refer to each particle's degeneracy and the function $S(m_{\perp}, p_{\perp})$ is given by Eq. (16). (Note that m_{\perp} is the same for Y^* and Y , but p_{\perp} varies).

Figure 3 shows the application of this procedure to the cases $(K^* + \bar{K}^*)/(K_S)$ (top), $\Sigma^*(1385)/\Lambda$ (middle), and η'/η (bottom) at two freeze-out temperatures and flows: $T = 140\text{MeV}, v_{max}/c = 0.55$ on left and $T = 170\text{MeV}, v_{max}/c = 0.3$ on the right. Significant deviations from simple constant values are observed, showing the sensitivity of the ratio to freeze-out geometry and dynamics. The analytically simple result in Eq. (18) is valid only if the light particle Y has been corrected for feed down from resonances, including Y^* . In other words,

Eq. (18) as well as Fig. 3 require that decay products from reconstructed Y^* do not appear on the bottom of the ratio. Experiments usually do not do such feed down corrections [19, 20, 21, 22], since this would increase both statistical and systematic error on the ratio, and it is not always possible to do such corrections at all (undetected decays) or in the full range of experimental sensitivity.

Introducing the feed down corrections into Eq. (18), we obtain

$$\frac{Y_{\text{observed}}^*}{Y_{\text{observed}}} = \frac{g^* S(m_\perp, p_\perp^*)}{g S(m_\perp, p_\perp) + \sum_i g_i^* b_{Y_i^* \rightarrow Y} R(m_\perp, p_{Ti})}. \quad (19)$$

Here, $S(m_\perp, p_\perp)$ describes the directly produced particles and has the form given by Eq. (15) and each term $R(m_\perp, p_{Ti}^*)$ describes a feed down contribution.

In the case of an incoherent many-particle system, such as that we are dealing with, the dynamical (matrix element) part of the decay amplitude factors out [49], and $R(m_\perp, p_{Ti}^*)$ is obtained by integrating the statistical hadronization distribution with a weight given by the phase space elements of the decay products. Thus, for a generic $Y^* \rightarrow Y$ feed down is given by an N -body decay,

$$R(m_\perp, p_\perp) = \int \prod_{j=2}^N \frac{d^3 p_j}{E_j} S(m_T^*, p_T^*) \delta \left(p_\mu^* - p_\mu - \sum_2^N p_{j\mu} \right), \quad (20)$$

where the integral is performed over the whole allowed region. If more than one feed down occurs, Eq. (20) can be used iteratively, with the left-hand side to be fed back to the right-hand side at each successive iteration.

In general, this expression can get very complicated, and the Monte Carlo integration becomes necessary. For most cases considered here, where there is one feed down and two or three body decays, Eq. 20 can be carried out semianalytically [17, 23, 24].

Figure 4 shows the ratios, including feed down of resonances, for the same particles and statistical hadronization conditions as were studied in Fig. 3. In the $\Sigma^*/(\text{all } \Lambda)$ case we omitted the feed down from Ξ to Λ which is usually corrected for (if this is not done the ratio $\Sigma^*/(\text{all } \Lambda)$ would depend strongly on the chemical potentials). We did allow for the $\phi \rightarrow K_S K_L$ feed down, since it is a strong decay that cannot so easily be corrected for. We note that the feed down from particles with a different chemical composition cannot always be corrected for, and thus some resonances ratios will also acquire a (mild) dependence on the chemical potentials. This is even true for ratios such as $\eta' / (\text{all } \eta)$, given different $s\bar{s}$ content, in this paper, these type chemical corrections were set equal to unity.

To further study the sensitivity of resonance-particle m_\perp -ratio to freeze-out dynamics, we also present the (feed down corrected) case as a function of p_\perp rather than m_\perp in Fig. 5. Unsurprisingly, we see grossly different behaviors, with many of the results coalescing. This of course is an expression of the fact that Y^* and Y have

dramatically different p_\perp at the same m_\perp and vice versa. We believe that the m_\perp ratio will in general be more sensitive to freeze-out dynamics, since its dependence on m_\perp is dominantly due to freeze-out geometry and dynamics. However, the p_\perp dependence seen in Fig. 5 provides an important self-consistency check for our previous results. We have found that the m_\perp ratios are often greater than unity even though there must be more ground state particles than resonances. Now it can be seen in the p_\perp ratio, that this requirement is satisfied.

IV. DISCUSSION

In general the the m_T and p_T dependence of the ratios in Fig 3 and, respectively, Fig 4 depends on freeze-out geometry and dynamics. Changes in temperature and flow velocity alter the shape. The introduction of a steeper flow profile will further raise all of the considered ratios, since a considerable fraction of particles will be produced in regions that do not flow as much. The effect of freeze-out dynamics will generally go in the same direction as freeze-out approaches the explosive limit ($dt_f/dr \rightarrow 1$). However, both the magnitude and the qualitative features of the two effects (flow and freeze-out velocity) will be considerably different. Especially, when more than one ratio is measured, it would appear that we will be able to determine the freeze-out condition. This is in contrast to the m_\perp distributions in Fig. 2, where the effects discussed in this paper result in linear corrections, which tend to compete, making the task of extracting the freeze-out dynamics much more ambiguous. Thus, there is considerable potential of resonance-particle m_\perp -ratios as a freeze-out probe.

The presence of a long living hadronic gas rescattering phase can distort our freeze-out probe. In particular, the apparent Y^*/Y ratio will be altered due to the depletion of the detectable resonances through the rescattering of their decay products. It's dependence on m_\perp will be affected in a non-trivial way, since faster (higher p_\perp) resonances will have a greater chance to escape the fireball without decaying, thus avoiding the rescattering phase altogether. Regeneration of resonances in hadron scattering may add another m_\perp dependence which is different for the Σ^*/Λ and the K^*/K ratios [50]. Other signals of the existence of such an interacting hadron gas phase have been considered [12, 23]. Fortunately, there is no evidence that a rescattering phase plays a great role in particle distributions. Even so, it would seem that the "safest" probes for freeze-out are the particles and resonances most unlikely to rescatter.

For this reason we have included the η'/η ratio in our considerations. $\eta \rightarrow \gamma\gamma$ and $\eta' \rightarrow \gamma\gamma$ have very different branching ratios, but have the same degeneracies and similar but rather small partial widths. The electromagnetic decay mode is practically insensitive to posthadronization dynamics. Regeneration effects are suppressed since the hadronic two body decay channel

is suppressed. All these features make these particles interesting probes, allowing for the analysis considered here. η, η' mesons have been measured at SPS energies in the $\gamma\gamma$ decay channel [47, 48], and detectors such as PHENIX are capable of reconstructing the same decays at RHIC.

While a long rescattering phase would affect the Σ^* distribution, the effect would be very easy to detect experimentally: 95% of Σ^* decay through the p -wave $\Sigma^* \rightarrow \Lambda\pi$ channel. However, regenerating Σ^* s in a gas of Λ s and π s is considerably more difficult, since $\Lambda\pi$ scattering will be dominated by the s -wave $\Lambda\pi \rightarrow \Sigma^\pm$. This situation will not occur for $K^* \leftrightarrow K\pi$, since both decay and regeneration happen through the same process, leading to a very fast reequilibration time [50]. Since both Σ^*/Λ and K^*/K ratios have been calculated within the thermal model [12] (neglecting rescattering), a strongly depleted Σ^*/Λ ratio (compared with K^*/K) suggests that a statistical freeze-out description, such as that given in this paper, is incomplete, and an interacting hadron gas phase is also necessary.

In summary, we have presented an overview of the different statistical freeze-out models used to fit heavy ion data. We have shown how the freeze-out geometry and freeze-out dynamics influences the hadron spectra. Our primary result is the finding that the m_\perp dependence of the resonance-particle ratios is a probe of freeze-out. We have presented these ratios for three particle species and two freeze-out conditions and have considered how our results could be altered by posthadronization phenomena.

Acknowledgments

Supported by a grant from the U.S. Department of Energy, DE-FG03-95ER40937. We thank Patricia Fachini (BNL) and Zhangbu Xu (Yale), from the STAR collaboration, as well as Marcus Bleicher (ITP-Frankfurt) for fruitful discussions.

-
- [1] E. Fermi, Prog. Theor. Phys. **5**, 570 (1950).
 - [2] I. Pomeranchuk, Proc. USSR Academy of Sciences (in Russian) **43**, 889 (1951).
 - [3] L. D. Landau, Izv. Akad. Nauk SSSR (Ser. Fiz.) **17**, 51 (1953); English edition, L. D. Landau, *Collected Papers of L. D. Landau*, edited by D. Ter Haar, Pergamon, Oxford (1965).
 - [4] R. Hagedorn, Suppl. Nuovo Cimento **3**, 147 (1965).
 - [5] J. Letessier and J. Rafelski, *Hadrons and Quark-Gluon Plasma* (Cambridge University Press, Cambridge, 2002).
 - [6] P. Braun-Muntzinger, I. Heppe and J. Stachel, Phys. Lett. B **465**, 15 (1999).
 - [7] L. Sandor, NA57 collaboration J. Phys. G in press, see <http://wa97.web.cern.ch/WA97/Publications.html> *Hyperon production at the CERN SPS: results from the NA57 experiment*
 - [8] F. Becattini, M. Gazdzicki and J. Sollfrank, Nucl. Phys. A **638**, 403 (1998); F. Becattini, J. Cleymans, A. Keranen, E. Suhonen and K. Redlich, Phys. Rev. C **64**, 024901 (2001) F. Becattini, J. Phys. G **28**, 1553 (2002).
 - [9] S.V. Afanasiev et. al., NA49 Collaboration, Nucl. Phys. A **715**, 161 (2003).
 - [10] G. Torrieri and J. Rafelski, New J. Phys. **3**, 12 (2001)
 - [11] S. V. Akkelin, P. Braun-Munzinger and Y. M. Sinyukov, Nucl. Phys. A **710**, 439 (2002)
 - [12] G. Torrieri and J. Rafelski, J. Phys. G **28**, 1911 (2002)
 - [13] J. Rafelski and J. Letessier, Nucl. Phys. A **715**, 98, (2003) J. Letessier and J. Rafelski, Int. J. Mod. Phys. E **9**, 107 (2000)
 - [14] J. M. Burward-Hoy, PHENIX collaboration, Nucl. Phys. A **715**, 498, (2003).
 - [15] J. Adams et al., STAR Collaboration, *Multi-Strange Baryon Production in Au-Au collisions at $\sqrt{s_{NN}} = 130$ GeV*, nucl-ex/0307024, submitted to Phys. Rev. Lett.
 - [16] K. A. Bugaev, M. Gazdzicki and M. I. Gorenstein, hep-ph/0211337.
 - [17] W. Broniowski and W. Florkowski, Phys. Rev. Lett. **87**, 272302 (2001)
 - [18] D. Magestro, J. Phys. G **28**, 1745 (2002)
 - [19] P. Fachini, STAR Collaboration, Nucl. Phys. A **715**, 462 (2003); J. Phys. G in press, nucl-ex/0305034; Haibin Zhang, STAR collaboration, J. Phys. G in press, nucl-ex/0305034;
 - [20] G. Van Buren, STAR collaboration, Nucl. Phys. A **715**, 129, (2003).
 - [21] C. Markert, STAR Collaboration, J. Phys. G **28**, 1753 (2002).
 - [22] V. Friese, NA49 Collaboration, Nucl. Phys. A **698** (2002) 487.
 - [23] G. Torrieri and J. Rafelski, Phys. Lett. B **509**, 239 (2001) and Phys. Rev. C **64**, 054907 (2001) Erratum-ibid. C **65**, 069902 (2002).
 - [24] E. Schnedermann, J. Sollfrank and U. W. Heinz, Phys. Rev. C **48**, 2462 (1993)
 - [25] E. Schnedermann, J. Sollfrank and U. W. Heinz, in Fireball spectra: *NATO Advanced Study Inst.: Particle Production in Highly Excited Matter, Il Ciocco, Italy, Jul 12-24, 1992*, H. Gutbrod and J. Rafelski, eds. proceedings series volume B303 (1993)
 - [26] U. W. Heinz and P. F. Kolb, Proceedings of the *18th Winter Workshop on Nuclear Dynamics* R. Bellwied, J. Harris, and W. Bauer, (EP Systema, Debrecen, Hungary, 2002), pp. 205-216 hep-ph/0204061
 - [27] F. Cooper and G. Frye, Phys. Rev. D **10** 186 (1974)
 - [28] K. A. Bugaev, Nucl. Phys. A **606**, 559 (1996)
 - [29] C. Anderlik et al., Phys. Rev. C **59**, 3309 (1999)
 - [30] D. Teaney, J. Lauret and E. V. Shuryak, Phys.Rev.Lett. **86** 4783 (2001).
 - [31] T. Susa, NA49 Collaboration, Nucl. Phys. A **698** (2002) 491.
 - [32] M. Gazdzicki, NA49 Collaboration, *proceedings of the*

- 30th International Workshop on Gross Properties of Nuclei and Nuclear Excitation: Hirscheegg 2002: Ultra-relativistic Heavy Ion Collisions, Hirscheegg, Austria, 13-19 Jan 2002* Edited by M. Buballa, W. Norenberg, B.-J. Schaefer, J. Wambach. Darmstadt, Germany, GSI, 2002. 377p. paper available as:
<http://theory.gsi.de/hirscheegg/2002/Proceedings/Gazdzicki>
 137.138.139.124 draft 1.ps.gz
- [33] S. V. Afanasiev *et al.*, NA49 Collaboration, J. Phys. G **28**, 1761 (2002).
 - [34] A. Olszewski *et al.*, PHOBOS Collaboration J. Phys. G **28**, 1801 (2002).
 - [35] P. Staszal *et al.*, Acta Phys. Polon. B **33**, 1387 (2002).
 - [36] J. D. Bjorken, Phys. Rev. D **27**, 140 (1983).
 - [37] P. J. Siemens and J. O. Rasmussen, Phys. Rev. Lett. **42**, 880 (1979).
 - [38] J. Letessier and J. Rafelski, J. Phys. G **28**, 183 (2002)
 - [39] J. Rafelski and J. Letessier, Phys. Rev. Lett. **85**, 4695 (2000)
 - [40] E. Schnedermann and U. W. Heinz, Phys. Rev. C **47**, 1738 (1993).
 - [41] S. Pratt, Nucl. Phys. **A715**, 389 (2003).
 A. Dumitru and R. D. Pisarski, Nucl. Phys. A **698**, 444 (2002)
 - [42] A. Keranen, J. Manninen, L. P. Csernai and V. Magas, Phys. Rev. C **67**, 034905 (2003)
 - [43] B. Touschek, Nuovo Cimento B **58**, 295 (1968).
 - [44] R. Hagedorn, I. Montvay, and J. Rafelski, in: *Hadronic Matter at Extreme Energy Density*, N. Cabibbo and L. Sertorio, Edts. (Plenum Press, New York 1980), pp. 49-148.
 - [45] G. Torrieri and J. Rafelski, J. Phys. G in press and about to be published, nucl-th/0305071; Ullrich Heinz, private communication
 - [46] M. M. Aggarwal *et al.*, WA98 Collaboration, Phys. Rev. Lett. **83**, 926 (1999)
 - [47] R. Albrecht *et al.*, WA80 Collaboration., Phys. Lett. B **361**, 14 (1995)
 - [48] A. Lebedev *et al.* [WA80 Collaboration.], Nucl. Phys. A **566**, 355C (1994).
 - [49] J. Sollfrank, P. Koch and U. W. Heinz, *Prepared for HIRSCHEGG '91: 19th International Workshop On Gross Properties Of Nuclei And Nuclear Excitations*. Edited by Hans Feldmeier. Darmstadt, Germany, GSI, 1991. 243p.
 - [50] M. Bleicher, Nucl. Phys. A **715**, 85, (2003).

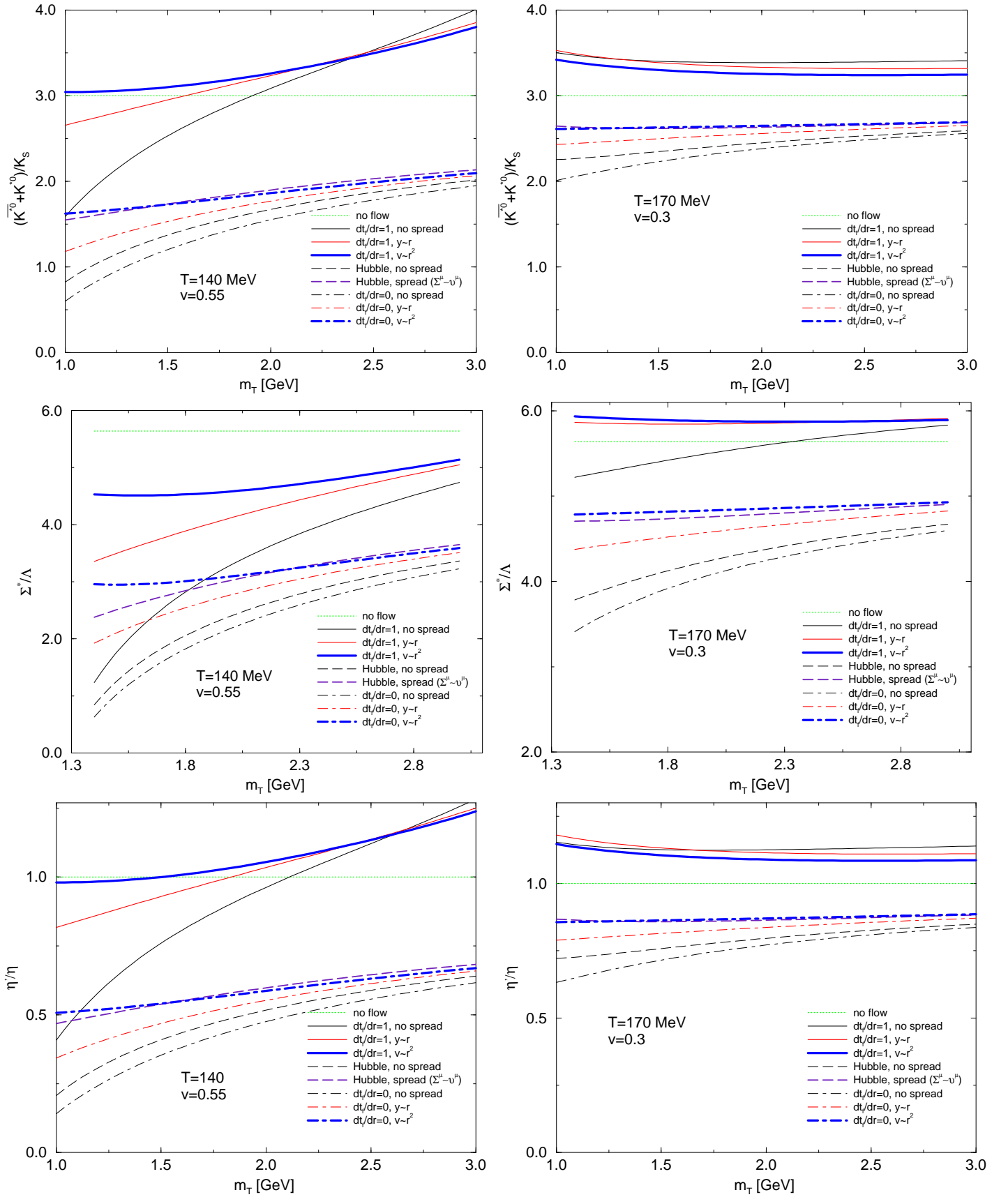


FIG. 3: (Color online) Dependence of the K^*/K , Σ^*/Λ and η'/η on the Freeze-out model .

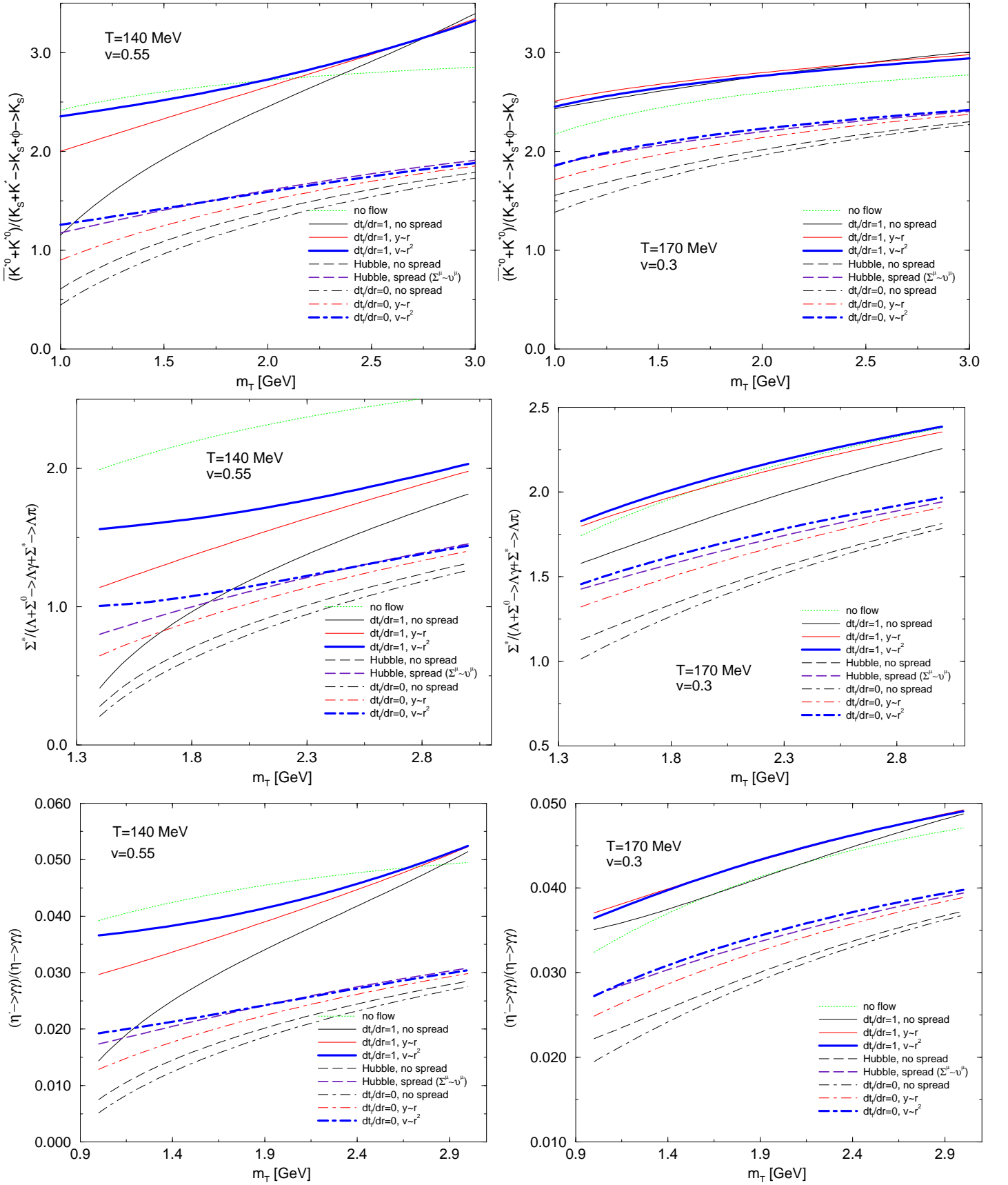


FIG. 4: (Color online) $(K^* + \bar{K}^*) / (\text{all } K_S)$, $\Sigma^*(1385) / (\text{all } \Lambda)$ and $\eta' / (\text{all } \eta)$ ratios, including feed down from resonances.

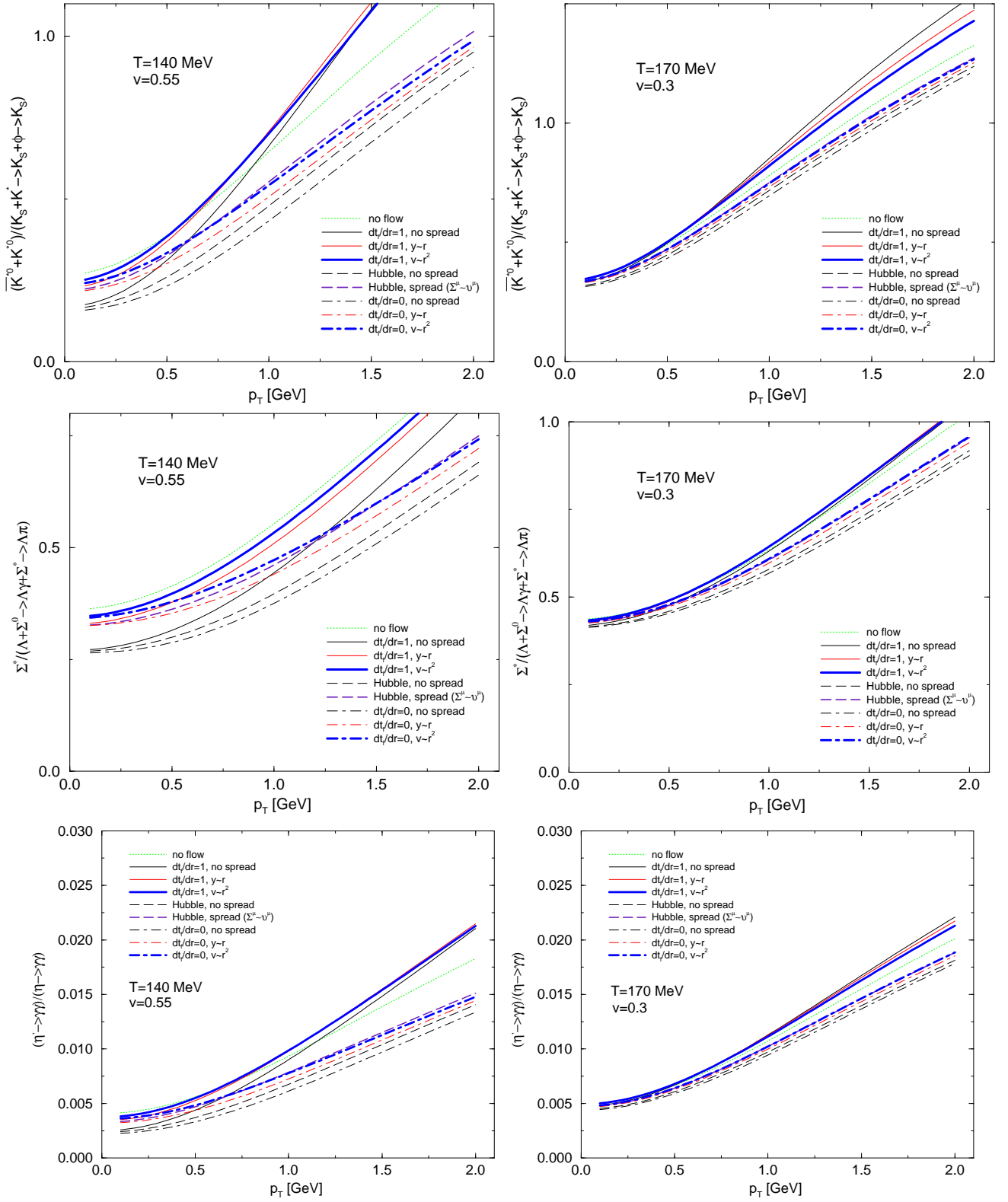


FIG. 5: (Color online) p_\perp dependence of $(K^* + \bar{K}^*)/(\text{all } K_S)$, $\Sigma^*(1385)/(\text{all } \Lambda)$ and $\eta'/(\text{all } \eta)$ ratios, including feed down from resonances.